INL/EXT-12-26708

First Results of Scanning Thermal Diffusivity Microscope (STDM) Measurements on Irradiated Monolithic and Dispersion Fuel

T. K. Huber
M. K. Fig
D. Garrett
J. R. Kennedy
A. B. Robinson
D. M. Wachs

July 2012

The INL is a U.S. Department of Energy National Laboratory
operated by Battelle Energy Alliance

Idaho National Laboratory

INL/EXT-12-26708

First Results of Scanning Thermal Diffusivity Microscope (STDM) Measurements on Irradiated Monolithic and Dispersion Fuel

T. K. Huber[1]
M. K. Fig
J. R. Kennedy
A. B. Robinson
D. M. Wachs

[1] Technische Universität München (TUM)

July 2012

Idaho National Laboratory
Originating Organization RERTR
Idaho Falls, Idaho 83415

http://www.inl.gov

Prepared for the
U.S. Department of Energy
Office of Nuclear Energy
Under DOE Idaho Operations Office
Contract DE-AC07-05ID14517

ABSTRACT

The evolution of thermal conductivity and related changes in thermal diffusivity during irradiation of research-reactor fuel plays a significant role in fuel element performance. To correctly simulate the heat fluxes and temperatures in the fuel meat during normal reactor operation, and also during potential accident scenarios, it is crucial to investigate the change in thermal conductivity and, thus, thermal diffusivity as a function of fission density and U-235 burnup.

The Idaho National Laboratory's (INL's) scanning thermal diffusivity microscope (STDM) was used to measure the thermal diffusivity of two irradiated monolithic U-10wt%Mo test plates having different burnup, and one irradiated dispersion U-7wt%Mo with a burnup profile similar to the high-burnup monolithic test plate. The measurement of the two monolithic U-10wt%Mo samples resulted in a mean thermal diffusivity of 4.5mm^2/s, which is significantly below non-irradiated U-10wt%Mo (6.4mm^2/s).

The STDM is a LASER-based instrument that measures the thermal diffusivity of irradiated fuel on a micrometer scale in a hot cell. Using the principle of photothermal deflection spectroscopy, the STDM focuses two concentric LASER beams onto the sample, one to heat the sample and the other for data-acquisition.

CONTENTS

FIGURES

TABLES

ACRONYMS

ATR	Advanced Test Reactor, Idaho
DU	depleted uranium
HEU	highly enriched uranium
HIP	hot isostatic press
INL	Idaho National Laboratory
LASER	Light Amplification by Stimulated Emission of Radiation
LEU	low-enriched uranium
RERTR	Reduced Enrichment Research and Test Reactors
STDM	Scanning Thermal Diffusivity Microscope
U-Mo	uranium-molybdenum (alloy)

First Results of Scanning Thermal Diffusivity Microscope (STDM) Measurements on Irradiated Monolithic and Dispersion Fuel

1. INTRODUCTION

The thermal conductivity of the fuel material in a reactor before and during irradiation is a sensitive and fundamental parameter for thermal hydraulic calculations that are used to correctly determine fuel-meat temperatures and to simulate performance of the fuel elements during operation. Several techniques have been developed to measure the thermal properties of fresh fuel to support these calculations, but it is crucial to investigate also the change of thermal properties during irradiation.

The scanning thermal diffusivity microscope (STDM) was developed at Idaho National Laboratory (INL) to be remotely operated in a hot cell to measure the thermal diffusivity of irradiated fuels [1]. Thermal diffusivity is, in addition to density and specific heat, the main parameter for determining thermal conductivity.

$$\lambda = \alpha \cdot \rho \cdot C_p \tag{1}$$

Results from the first STDM measurements of two monolithic U-10wt%Mo and one dispersion U-7wt%Mo mini-plate will be presented in the following sections. As part of destructive post-irradiation examination, the thermal diffusivity of the three samples has been determined using the INL STDM.

1.1 Theory

When a pulsed laser beam is incident on a material surface, the material absorbs some of the light and, in the process, converts light energy into thermal energy. This increase in thermal energy causes the material to undergo a local thermal expansion that is proportional to the energy absorbed. If the time between laser pulses is sufficiently large, the locally absorbed thermal energy will diffuse throughout the body of the material according to the diffusion equation for heat conduction. As the volume of absorption cools, it undergoes thermal contraction, the inverse of thermal expansion. If, on the other hand, the time between the laser pulses is sufficiently small, the material will not be able to diffuse the thermal energy absorbed during each pulse before more energy is absorbed. This will result in a continued local thermal expansion.

It is reasonable to postulate that there exists a unique pulse frequency, called the cut-off frequency, between these two extremes which will allow the material to maintain a balance between the diffusion of thermal energy from the preceding pulse, tending to cause thermal contraction, and the absorption of energy during the current pulse, tending to cause thermal expansion. In this equilibrium, the material will be in a quasi-steady thermally expanded state. It is this unique frequency that the STDM finds.

This process of expansion and contraction is controlled by a coupling of the thermal and elastic properties of the absorbing material. By solving the coupled equations and simplifying when necessary, it can be shown that the cut-off frequency (f_c) of the material is proportional to ratio of the thermal diffusivity (D) to the square of the laser spot size (a), and that the proportionality constant is independent of the material.

$$f_c \propto \frac{D}{a^2} \tag{2}$$

If the frequency of the laser pulses is allowed to vary from a starting point of several hundred Hz upward, the cut-off frequency can be detected by a second laser that measures the expansion and contractions of the material surface. If the cut-off frequency for several materials of known thermal

diffusivity is obtained in this way by the STDM, a log-log plot of the above equation for all of the materials will be linear. This plot can then be used as a calibration curve for finding the thermal diffusivity of an unknown material.

2. FUEL PLATE CHARACTERISTICS AND IRRADIATION

2.1 Monolithic Samples

For the STDM measurement, two monolithic mini plates (L1P12Z and L2P16Z) from the RERTR 10A experiment [2] were chosen for analysis. The RERTR-10A irradiation experiment was designed to evaluate the performance of monolithic fuel designs of various types under severe irradiation conditions (surface heat flux >400 W/cm^2 and burnup >100% LEU equivalent). The experiment was also designed to provide a basis to examine the performance of the fuel meat to cladding interface when a Zr interlayer with either 0.025mm or 0.050mm nominal fuel-foil thickness was inserted to mitigate U-Mo/Al inter-diffusion during irradiation. These two specific plates were selected because they offered the opportunity to examine the impact of a wide range of fission densities on thermal diffusivity.

Each plate is nominally 2.54cm wide, 10.1cm long, and 1.4mm thick. All plates in the experiment were fabricated by first casting uranium-molybdenum alloy ingots by arc melting, then hot rolling the ingots into thin foils and subsequently using the hot-isostatic-press (HIP) method to bond the cladding to the fuel core.

The uranium-molybdenum fuel alloy of plate L1P12Z has an enrichment of 67.0% U-235 and contains 10.1wt% Mo. The fuel foil with an average thickness of 0.310mm has a co-rolled 0.025mm Zr interlayer and is clad in Al-6061. Plate L2P16Z contains a 33.4% U-235 enriched fuel foil with 10.1wt% Mo, has a 0.025mm co-rolled Zr interlayer and is also clad in Al-6061 [3]. The average foil thickness is 0.536mm. This variation in thickness and enrichments allowed the plates to be irradiated at similar temperatures while simultaneously achieving different fission rates (which led to a variation in average fission density at the end of irradiation, see 2.3).

2.2 Dispersion Sample

The R6R018 fuel plate [4] of the RERTR-9B experiment [5] was chosen as a representative dispersion fuel-meat sample for STDM examination. The goal of this irradiation program was to investigate the impact of Si addition to the matrix material of dispersion U-7wt%Mo fuels under irradiation. Variations in the Si content in the fuel meat can substantially alter the volume fraction of U-Mo/Al interaction-product formation. As such, it is anticipated that significant variation in bulk thermal diffusivity will be observed. This plate has the same nominal dimensions as the RERTR 10A mini-plates.

The fuel powder was produced by first alloying a blend of highly enriched uranium (HEU – 93.1wt% U-235), depleted uranium (DU – 0.20wt% U-235) and molybdenum by arc-melting, in the end producing a total enrichment of 62.5% U-235 and a molybdenum content of 6.99wt%. The alloy was subsequently atomized by the rotating-electrode atomization process. A blend of 5.540g of fuel powder and 0.921g gas-atomized aluminium powder with 3.5wt% Si content was compacted in a hydraulic press. These fuel compacts were loaded into machined Al-6061 “picture frames” with cover plates and rolled in a two-high rolling mill. The rolling assembly was periodically reheated with a plate-heating furnace at 500°C. Finally, the plate was annealed at 485°C for 30 minutes and, afterwards, cooled in air. During this process, silicon in the matrix material accumulates around the fuel particles. This Si-rich layer was expected to reduce the diffusion of uranium into the matrix during irradiation, which typically leads to the growth of a disadvantageous inter-diffusion layer around the U-Mo particles.

2.3 Irradiation

RERTR mini-plate experiments [2], [5] consist of four capsules labelled from A to D, each containing eight mini-plates. RERTR-10A, consisted of the two capsules, A and C, with plate L1P12Z located in position C1 and plate L2P16Z in position C3. RERTR-9B consisted of the two capsules B and D, with plate R6R018 in position B7.

The plates are arranged in two rows of four in each capsule. Both experiments were irradiated in the B-11 position of the Advanced Test Reactor (ATR), with the capsule oriented such that one edge of the plates is facing the core centre (see Figure 1). The orientation combined with the higher enrichment leads to self-shielding and a subsequent large fission-density gradient across the 2.54cm width of the plate [2].

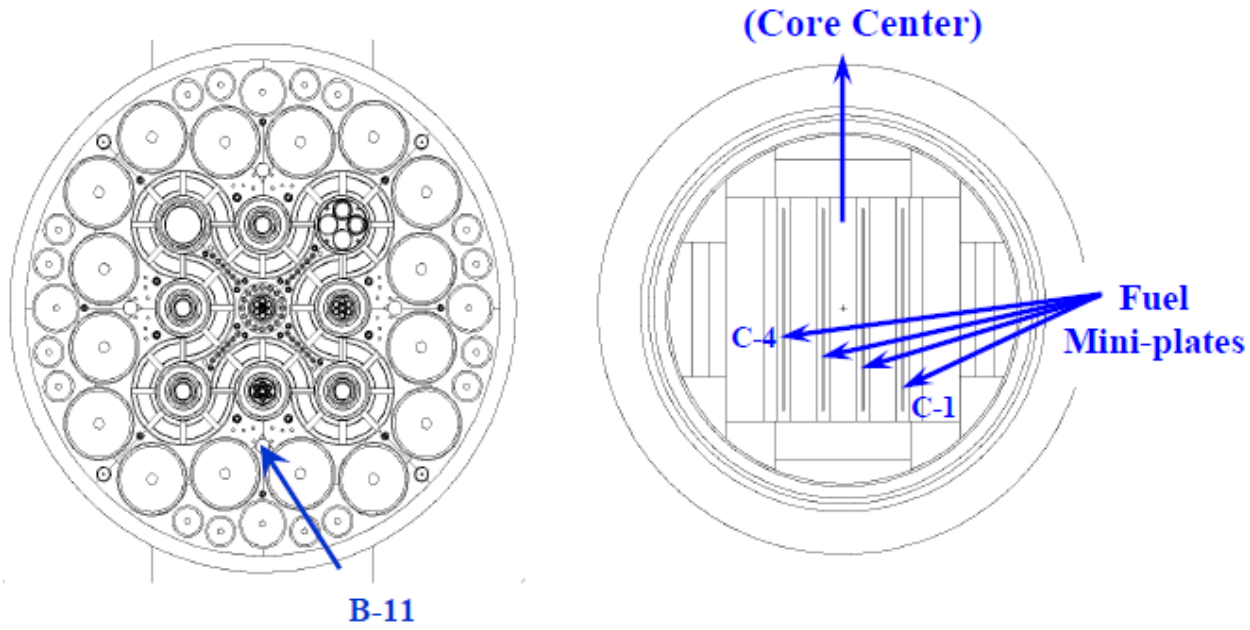

Figure 1: (left) Radial cross section of ATR core, (right) assembly orientation in the irradiation position.

The RERTR-10A plates were irradiated during cycles 142B and 143A for 52d and 26d [2], respectively, and the RERTR-9B plates were irradiated during cycles 140A, 140B and 141A for 46.5d [5], 35d and 32d, respectively. Table 1 shows the plate-specific average fission density and U-235 burnup at the end of irradiation.

Table 1: Average fission density and U-235 burnup after irradiation.

	Plate Average Fission Density in meat [f/cc]	**Plate Average U-235 Burnup [%]**	
L1P12Z	4.04·1021	21.96	monolithic
L2P16Z	1.91·1021	19.14	monolithic
R6R018	3.49·1021	34.02	dispersion

Figure 2 and Figure 3 show the power and fission-density gradients across the width of the samples obtained by neutronic physics analysis.

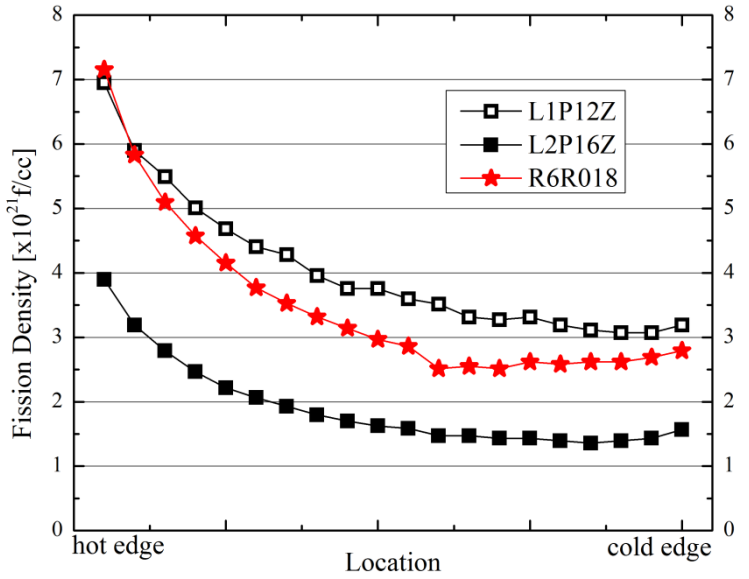

Figure 2: Localised fission density across samples.

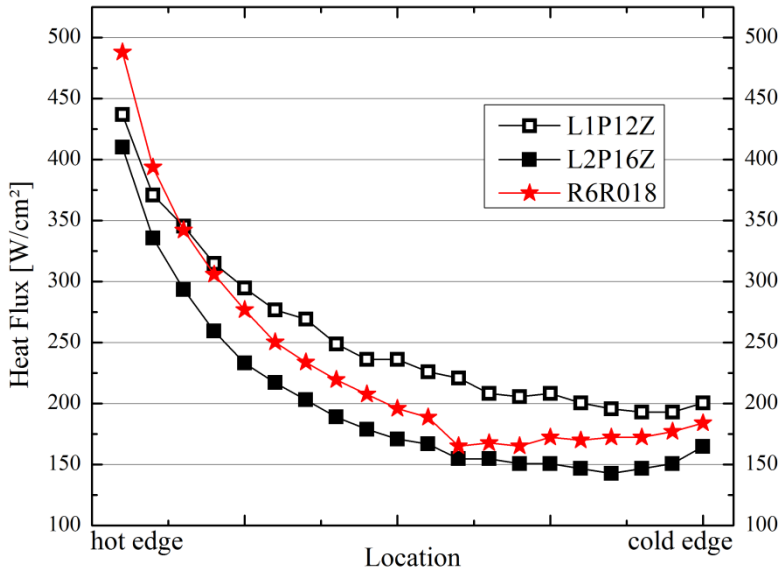

Figure 3: Localized heat flux across samples.

Post-irradiation thickness measurements for plates L1P12Z and L2P16Z were performed as described in Figure 4. The results, including pre-irradiation plate thicknesses and pre-irradiation foil thicknesses, can be found in Table 5 and Table 6 in Appendix A.

Table 7 in Appendix A shows the results of the thickness measurements of plate R6R018 before and after irradiation. Calculations [4] based on fission density across the plate width (nominal width, 3.995±0.020 in.) in the area of the STDM mount lead depending on the burn-up to a fuel meat swelling of 15% to 48% due to gaseous and solid fission products.

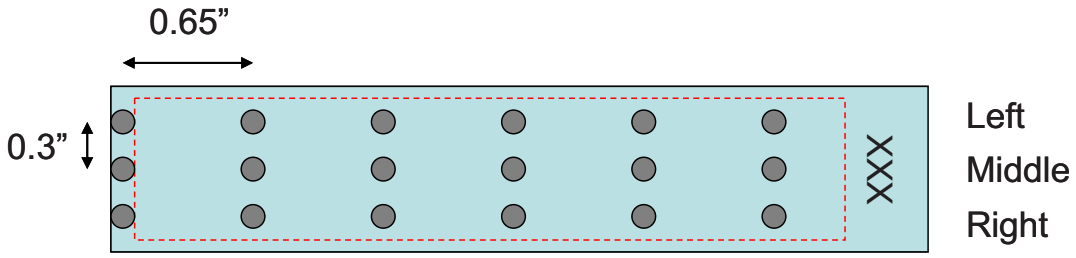

Figure 4: Thickness measurement locations over fuel plates.

A cross section was taken through the mid-plane of each irradiated fuel plate for STDM examination (see Figure 5).

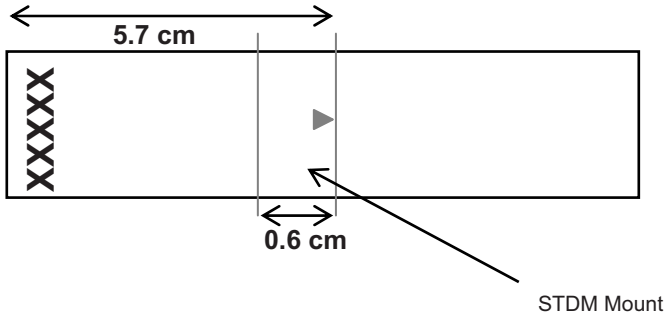

Figure 5: Sectioning diagram for STDM samples.

3. EXPERIMENTAL

3.1 Results

Due to the different material structure and behaviour under irradiation, the monolithic and dispersion samples show different results in the STDM and are therefore examined in separate sections below.

3.1.1 Monolithic samples

Figure 6, Figure 7 and Figure 8 show a map of the measured thermal diffusivity across the width of both monolithic plates L1P12Z and L2P16Z. On the left and right side of the diagrams one can see the thermal diffusivity of the cladding material and of the fuel zone in the middle of the plates, with a characteristic low thermal diffusivity.

The L1P12Z sample was measured twice, and the values shown in Table 2 are the average of both measurements.

Table 2: Thermal diffusivity values[a] for cladding and fuel zone of both monolithic plates compared to values of a previous STDM and LASER Flash measurement of a fresh U-10wt.%Mo fuel plate sample.

	L1P12Z	**L2P16Z**	**Fresh Material (STDM)**	**Fresh Material (LASER Flash) [4]**
Al-6061	(47.3 ± 0.9)mm²/s	(45.7 ± 1.3)mm²/s	(50.3 ± 6.0)mm²/s	
U-10wt%Mo	(4.93 ± 0.73)mm²/s	(4.06 ± 0.63)mm²/s	(6.4 ± 0.8)mm²/s	(4.8 ± 0.3)mm²/s

[a] The uncertainty for each data point is 12%. The average values have been weighted by the uncertainty of each data point.

It is remarkable that the value for the fresh fuel, obtained by using the LASER-flash method, is lower than the one using the STDM. But the LASER-flash sample has a different fabrication history, as it was cut from a cast pin. Thus, it has a different microstructure and heat treatment than the plate-type samples used for STDM measurements. This impact of different heat treatment and microstructure on thermal diffusivity has been experimentally observed on pin-type samples [7].

Regarding the thermal diffusivity of Al-6061 cladding, the values of the irradiated material are lower than for fresh material. Although aluminum is known for its low activation during irradiation, the highly energetic fission products and neutron irradiation, especially fast neutrons, cause microstructural damage in the cladding material and, thus, decrease its thermal diffusivity.

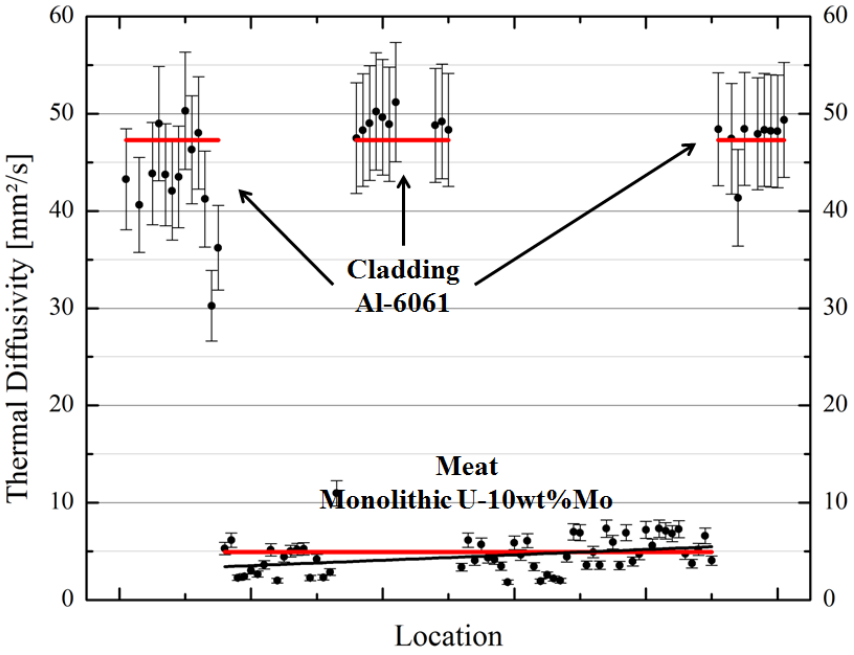

Figure 6: First thermal diffusivity map across the width of plate L1P12Z. The red lines are the mean values of Al-6061 and U-10wt%Mo (see Table 2). The black line is fitted to show the gradient in the thermal diffusivity of the meat along the width of the plate.

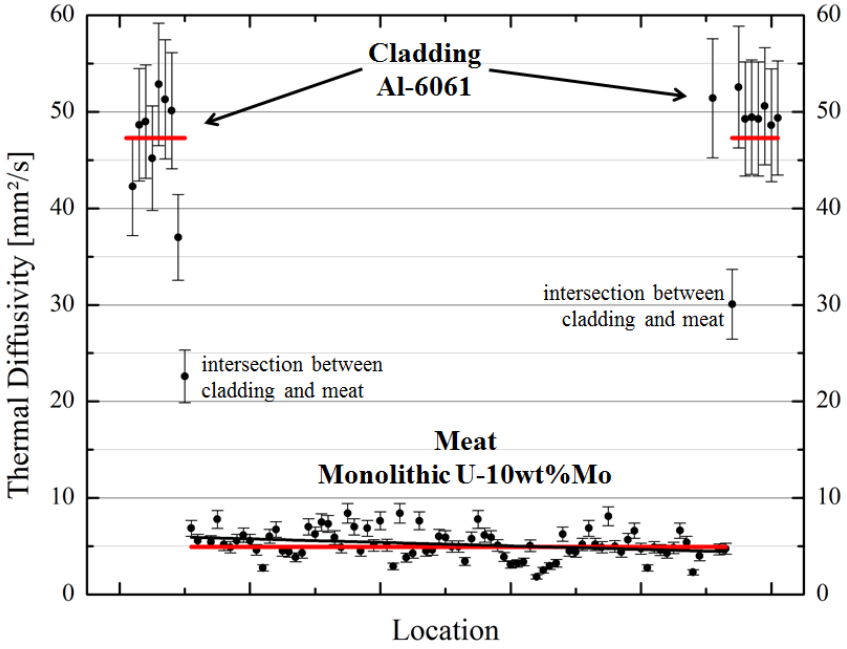

Figure 7: Second thermal diffusivity map across the width of plate L1P12Z. The red lines are the mean values of Al-6061 and U-10wt%Mo (see Table 2). The black line is fitted to show the gradient in the thermal diffusivity of the meat along the width of the plate.

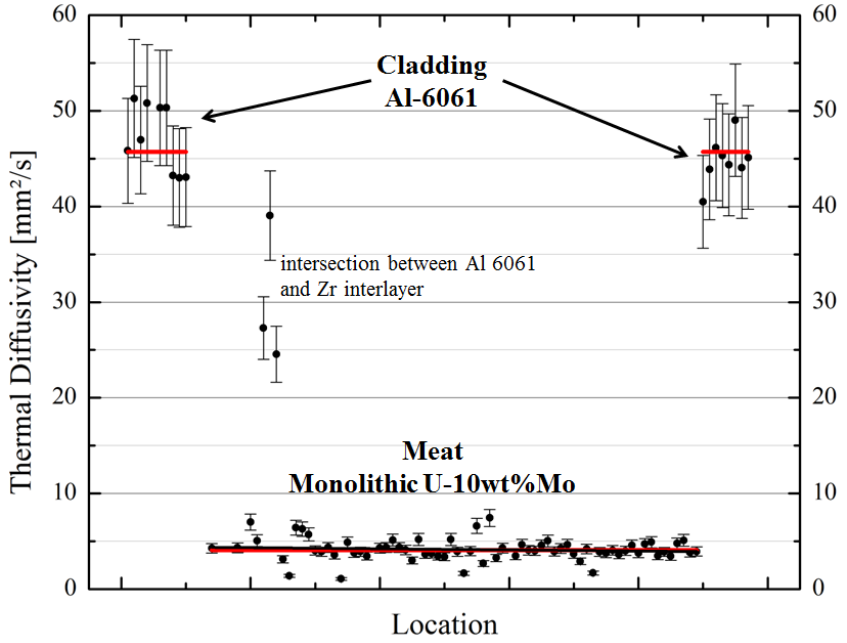

Figure 8: Thermal diffusivity map across the width of plate L2P16Z. The red lines are the mean values of Al-6061 and U-10wt%Mo (see Table 2). The black line is fitted to show the gradient in the thermal diffusivity of the meat along the width of the plate. But in contrast to plate L1P12Z, no significant gradient can be observed.

The map of plate L1P12Z shows data points around 20mm²/s to 30mm²/s at the intersection between cladding and fuel zone. There, at the boundary, the STDM measures a mixture of both materials, as the LASER beam encloses an area of ~50µm diameter. The signal determines a combined value for the

highly conductive Al-6061 and the less conductive U-10wt%Mo, varying with the enclosed volume fraction of each material.

On the map of plate L2P16Z are three strongly deviating points in the meat zone. Taking into account the literature value for the thermal diffusivity of Zr (12.6mm²/s) [8], these points are, again, likely the result of a boundary measurement, namely between the Zr barrier and the cladding material. The reason for the deviations from the meat zone is that the measurement location is controlled through a lens that degrades and tarnishes due to radiation damage. Thus, the measurement location can drift to boundaries, smear over, and lead to deviations from the fuel zone. This can be clearly observed in Figure 6, where the operator drifted into the cladding zone on the rim of the meat zone.

Further, plate L1P12Z shows in the first measurement (Figure 6) a clear gradient in the thermal diffusivity of the meat as a function of location. A slighter gradient can also be observed on the second measurement, while plate L2P16Z shows no significant gradient. Regarding the burnup, L1P12Z has a higher burnup in total and a steeper gradient than L2P16Z. It can therefore be assumed that thermal diffusivity depends on the burnup in the fuel. But which side of the sample experienced the high burnup is not known; thus, dependence on burnup cannot be proven at this point.

Besides the thermal diffusivity α, the density ρ and specific heat C_p of the materials are factors that must be known for the calculation of thermal conductivity λ (see

Table 3). The density of the meat changes during irradiation (compare the hot and cold edges of the plates in Figure 9 and Figure 10). It is assumed that there is no significant change in the specific heat because no data exist as yet describing how it might change. Density change depending on the fission density f_D was examined in the RERTR-12 experiment [12] by weighing the fuel plate in air and in water before and after irradiation. The relative density change $\Delta\rho$ is calculated using equation (2) and leads to -2.5% for plate L1P12Z and -1.2% for plate L2P16Z.

$$\Delta\rho = (-6.07 \pm 0.32) \cdot 10^{-24}[cc/f] \cdot f_D \quad (2)$$

Table 3: Thermophysical properties for Al-6061 [5] and non-irradiated U-10wt.%Mo [4].

	Density @300K	**Specific Heat @300K**
Al-6061	2.7g/cm³	0.896J/gK
U-10wt.%Mo	16.75g/cm³	0.134J/gK

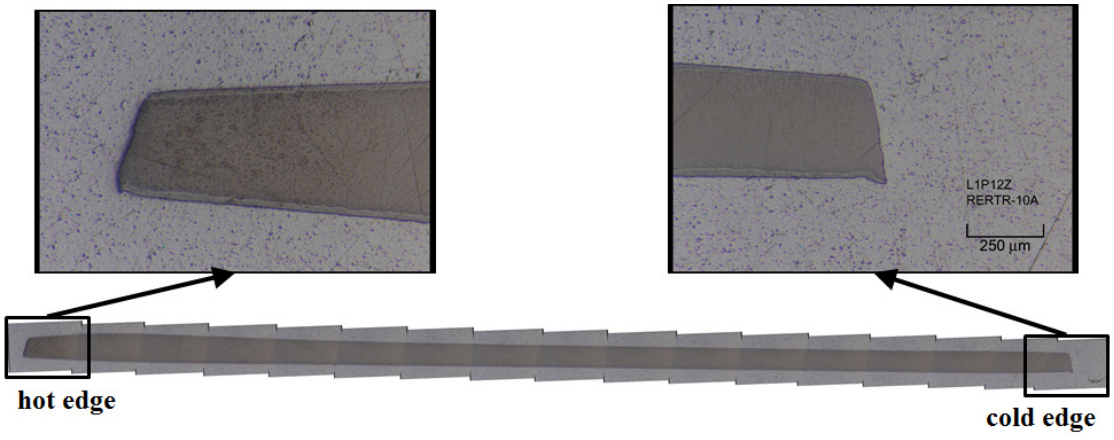

Figure 9: Post-irradiation optical-microscope picture of plate L1P12Z with magnification of the hot and cold edges of the meat zone.

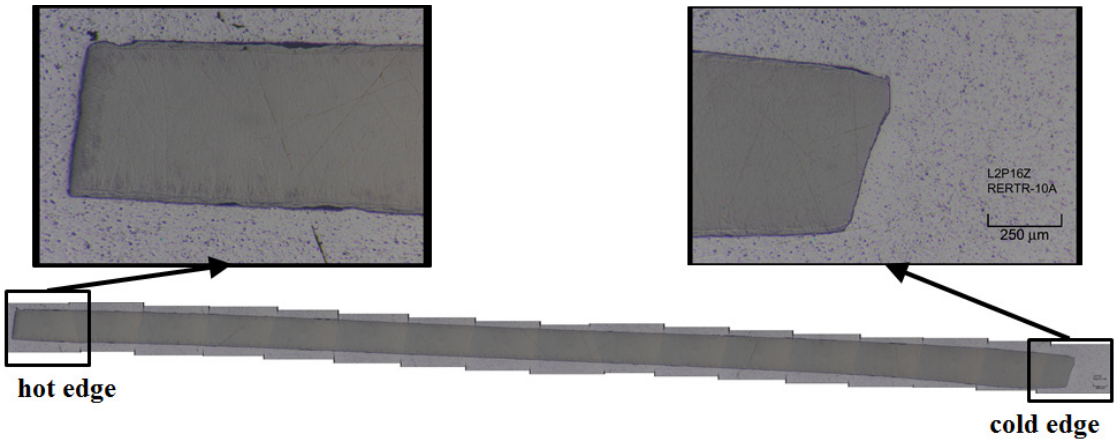

Figure 10: Post-irradiation optical-microscope picture of plate L2P16Z with magnification of the hot and cold edges of the meat zone.

Using formula (1) and the information given in

Table 3, it is possible to estimate the thermal conductivity of the irradiated U-10wt.%Mo fuel and Al-6061 cladding. When calculating the thermal conductivity of the irradiated meat, the change in the density has to be considered using formula (3).

$$\rho_{meat} = \rho_{U-10wt.\%Mo} \cdot (1 + \Delta\rho) \tag{3}$$

Table 4: Thermal Conductivity for irradiated monolithic U-10wt%Mo and Al-6061 compared to non-irradiated STDM and literature data.

	U-10wt%Mo	**Al-6061**
L1P12Z irradiated	(9.0 ± 1.5)W/mK	(114.4 ± 2.1)W/mK
L2P16Z irradiated	(10.9 ± 1.7)W/mK	(110.6 ± 3.2)W/mK
Non-irradiated (STDM)	(14.4± 1.9)W/mK	(121.6 ± 15.0)W/mK
Non-irradiated @300K [4], [5]	11.1W/mK	167W/mK

The thermal conductivity of fresh Al-6061 measured by the STDM is far below the literature value. During the HIP process, the plates are heat treated and pressurized, which can have an impact on the thermal diffusivity and, consequently, on the thermal conductivity of the aluminium alloy. Comparing the different tempers of Al-6061, the thermal conductivity ranges between ~150W/mK and ~180W/m/K.

3.1.2 Dispersion Samples

Figure 11 presents a map of thermal diffusivity across the width of the dispersion fuel plate R6R018.

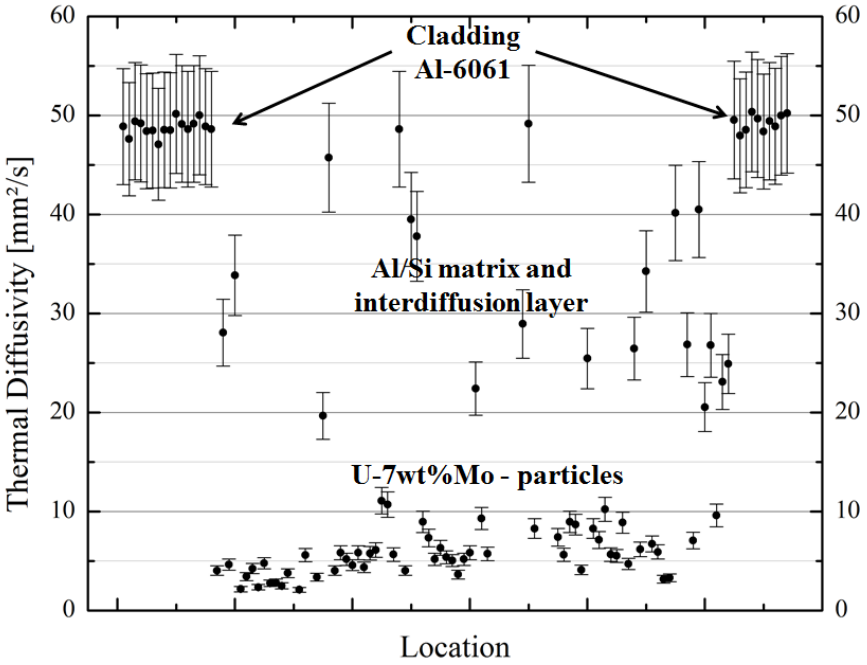

Figure 11: Thermal diffusivity map across the width of plate R6R018.

Again both sides of the diagram show the thermal diffusivity of the Al-6061 cladding. In the fuel-meat zone, the low diffusivity (<10mm²/s) indicates U-7wt%Mo particles. The spikes up to thermal diffusivity values of the cladding are caused by the fuel structure (see Figure 12), an alternation of fuel particles and matrix material.

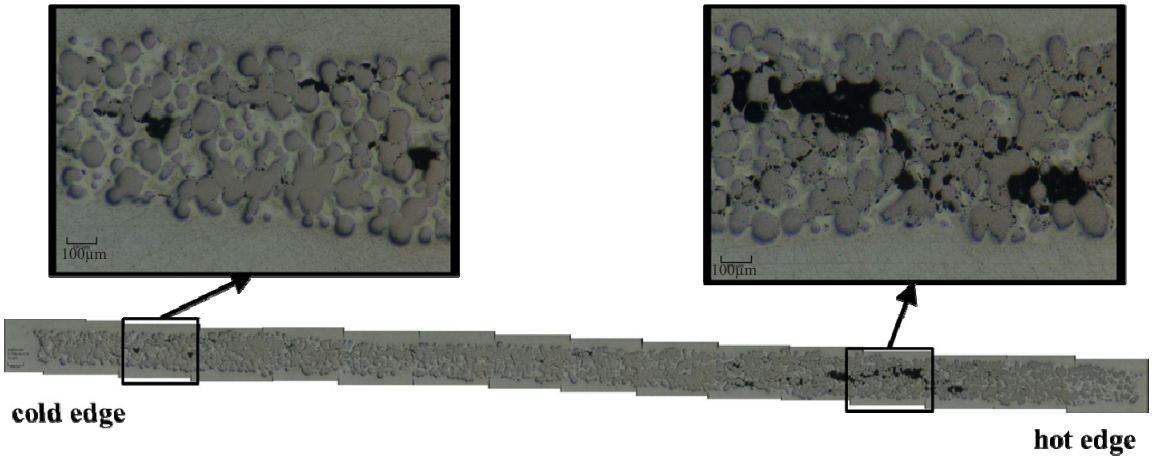

Figure 12: Post-irradiation optical-microscope picture of plate R6R018 with magnification of the hot and cold edges of the meat zone.

Compared to the measurement of the monolithic fuel plate L1P12Z, which has almost the same burnup but contains ~3% less highly conductive molybdenum (138W/mK) [9], a thermal diffusivity of <3.7mm²/s in the meat zone is expected. Indeed a few data points can be found within that low-diffusivity range. They result from measurements in which the LASER beam of the STDM directly hits a U-7wt%Mo particle such that the whole radius (~50µm) of the LASER beam covers the particle, which has a size of up to 106µm. In this case, the thermal diffusivity of the fuel particle itself is measured.

As already mentioned in the description of fuel production, the Si rich layer around the fuel particles reduces, but does not completely prevent the growth of an interdiffusion layer between the fuel particle and the Al matrix during irradiation. Figure 13, a magnification of the high-burnup zone, clearly shows a layer around the fuel particles, together with a destabilizing and low- to non-thermal conductive conglomeration of fission-gas voids.

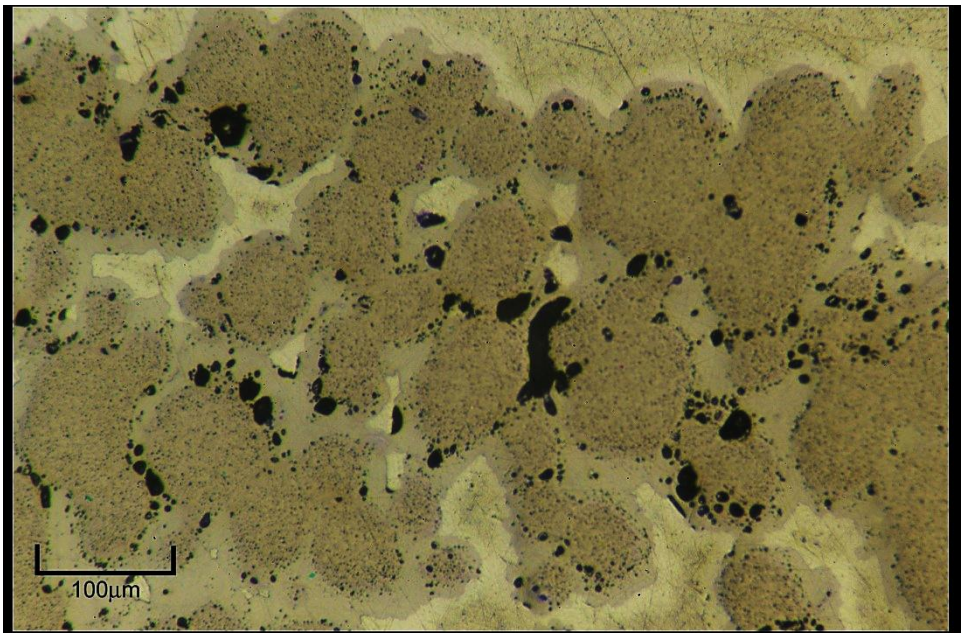

Figure 13: Post-irradiation optical-microscope magnification of the fuel particles with interdiffusion layer and fission-gas accumulations in the high burnup area.

Regarding the scale on the microscope picture, there are few locations where the diffusion layer has a thickness of >50µm, which minimizes the chance to measure only this layer as is the case for the bigger fuel particles. Instead either a mixture of diffusion layer and fuel particle or diffusion layer and matrix is measured. As the matrix consists of pure aluminum and silicon, which are high thermal-conductivity materials with thermal diffusivities of 97mm²/s for pure aluminum [10] and 88mm²/s for silicon [10], the composite thermal diffusivity must be within that range. However, the diagram shows only diffusivities below 50mm²/s, which indicates that only mixtures of the matrix with the less conductive diffusion layer or fuel particle have been measured.

Only taking into account the data points below 10mm²/s, those which indicate fuel particles or mixtures containing mostly fuel particles, again a gradient exists that could indicate a fission-density-dependent thermal diffusivity, just as has been seen in monolithic fuel.

This measurement of the dispersion fuel can only give qualitative statements concerning general thermal-diffusivity gradients depending on the burnup. It is not possible to calculate precise values for the fuel particles, inter-diffusion layer or matrix material as there is no information on the precise measurement location that could precisely identify the LASER-beam-enclosed materials.

3.2 Thermal Diffusivity Variation

Figure 14 shows the frequency of the data points according to a certain thermal diffusivity per fuel plate. The monolithic samples show a clear maximum in the fuel zone, with thermal diffusivities between 0mm²/s and 10mm²/s (see zoom–in on Figure 14) and the cladding zone above 40mm²/s. The thermal diffusivity of the dispersion sample is more scattered also between fuel and cladding zone due to the meat

structure, where mixtures between the highly conductive matrix material and the less conductive fuel have been measured.

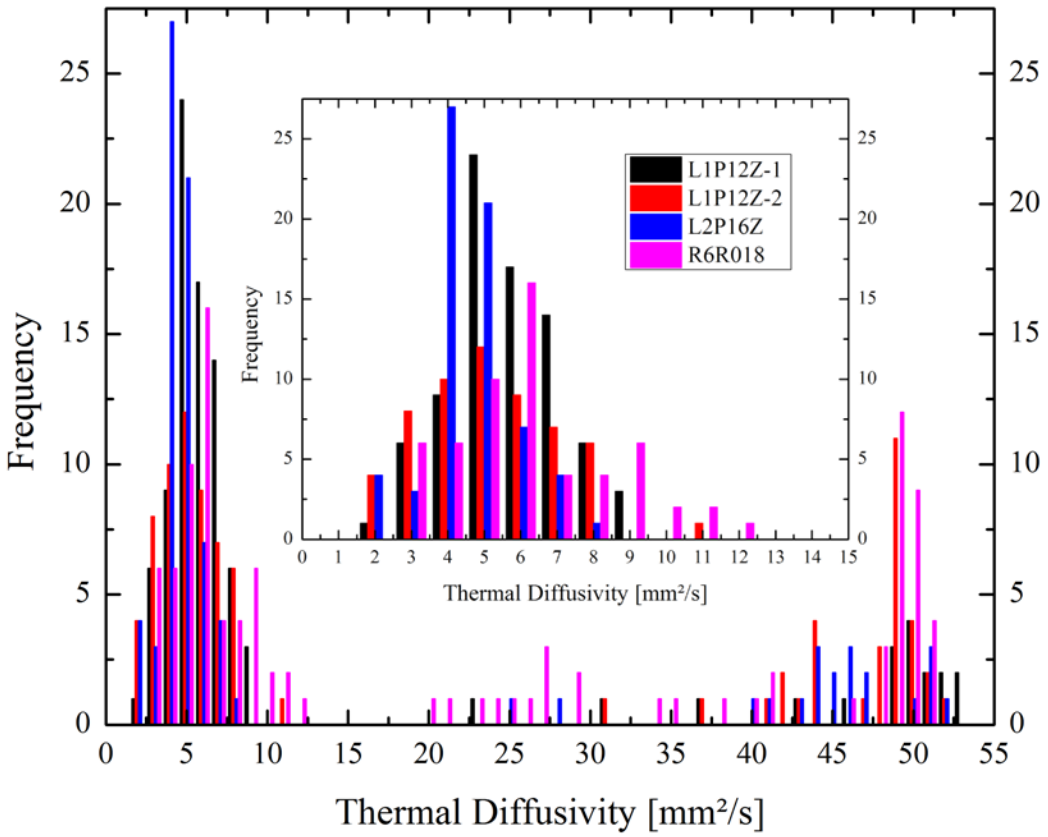

Figure 14: Frequency of the number of data points for certain thermal diffusivities per plate. The zoomed–in portion shows the meat zone between 0mm²/s and 15mm²/s.

4. CONCLUSION

The measurements of the monolithic samples show a mean thermal diffusivity of (4.5 ± 0.7)mm²/s, which is significantly lower than the STDM of fresh monolithic U-10wt%Mo of (6.4 ± 0.8)mm²/s.

A slight gradient has been observed over the width of plate L1P12Z, with, in total, a higher fission density and a steeper fission-density gradient, which can be an indication of a fission–density or burn-up dependent thermal diffusivity. No gradient was observed for L2P16Z. Additional samples should be evaluated to further study this behavior.

The mean thermal conductivity of the irradiated monolithic fuel was estimated to be (9.9 ± 1.6)W/mK, which is significantly lower than the thermal conductivity of fresh U-10wt%Mo (14.4 ± 1.9)W/mK, which is in good accordance with thermal conductivity measurements of fresh monolithic U-8wt.%Mo obtained by using the LASER flash method [11]. Thermal diffusivity is not the only parameter in the thermal conductivity calculation that changes during irradiation. The main parameter with the highest deviation is density; this, therefore, has the highest impact on thermal conductivity. Again it is mandatory to have exact information from the STDM measurement position combined with data on local fuel swelling to increase accuracy.

The change in specific heat during irradiation, which is currently assumed not to be significant, is still an unknown parameter without experimental determination.

The measurements performed on the dispersion fuel plate shows the high resolution of the STDM instrument. It is possible to separate fuel particles from the matrix. However, due to the lack of information on exact measurement position, it is not possible to give exact values for the thermal conductivity of single materials as overlapping measurements between two materials can occur.

The STDM is a powerful instrument, with very high resolution and accuracy in thermal diffusivity. However, it is necessary to improve the exact determination of the measurement position on the sample, especially for work with dispersion fuels.

5. ACKNOWLEDGEMENT

The authors are appreciative of the staff of the Hot Fuel Examination Facility and the Analytical Laboratory at the Materials and Fuels Complex of Idaho National Laboratory.

6. REFERENCES

[1] M. K. Fig, J. R. Kennedy, "Micro-Scale Thermal Diffusivity Measurements on Irradiated Nuclear Fuel", INL/LTD-11-23214, September 2011.

[2] D. M. Perez, M. A. Lillo, G. S. Chang, G. A. Roth, N. E. Woolstenhulme and D. M. Wachs, "RERTR-10 Irradiation Summary Report", INL/EXT-10-18456, May 2011.

[3] F. J. Rice, G. A. Moore, "RERTR-10 As-built Summary Report", INL/EXT-12-26721, July 2012.

[4] A. B. Robinson, D. M. Wachs, D. D. Keiser, P. G. Medvedev, C. R. Clark, G. S. Chang, M. A. Lillo, J. F. Jue, G. A. Moore and J. M. Wight, "Results of the Irradiation of R6R018 in the Advanced Test Reactor", INL/EXT-10-18074, April 2010.

[5] D. M. Perez, M. A. Lillo, G. S. Chang, G. A. Roth, N. E. Woolstenhulme and D. M. Wachs, "RERTR-9 Irradiation Summary Report", INL/EXT-10-18421, May 2011.

[6] D. E. Burkes, C. A. Papesch, A. P. Maddison, T. Hartmann and F. J. Rice, "Thermophysical properties of DU-10wt.%Mo alloys", J. Nucl. Mater. **403**, 160 (2010).

[7] J. T. Creasy, Master Thesis, Texas A&M University, 2011

[8] J. K. Fink and L. Leibowitz, "Thermal conductivity of zirconium", J. Nucl. Mater. **226**, 44 (1995).

[9] E. P. Mikol, *The Thermal Conductivity of Molybdenum over the Temperature Range of 1000-2100°F* (Oak Ridge National Laboratory, Oak Ridge – Tennessee, 1952), p. 1.

[10] J. E. Jensen, W. A. Tuttle, R. B. Stewart, H. Brechna and A. G. Prodell, *Brookhaven National Laboratory Selected Cryogenic Data Notebook* (Brookhaven National Laboratory Associated Universities Inc., United States Department of Energy, 1980), p. XV-A-1.

[11] R.M. Hengstler, L. Beck, H. Breitkreutz, C. Jarousse, R. Jungwirth, W. Petry, W. Schmid, J. Schneider, N. Wieschalla, "Physical Properties of Monolithic U8 wt.%-Mo", J. Nuc. Mat. **402** (2010).

[12] A. B. Robinson, F. J. Rice, M. K. Meyer, D. M. Wachs, D. D. Keiser, D. M. Perez, "Post Irradiation Examination Results of the RERTR-12 Campaign", In Proceedings of the 34th International Meeting on Reduced Enrichment for Research and Test Reactors (RERTR), 2012.

Appendix A

Table 5: Thickness measurements for L1P12Z [1]

POST IRRADIATION						
TOP	1.450	1.559	1.531	1.507	1.534	1.625
MIDDLE	1.454	1.558	1.566	1.538	1.577	1.683
BOTTOM	1.441	1.605	1.585	1.579	1.630	1.746
PRE-IRRADIATION						
TOP	1.4478	1.4478	1.42494	1.39192	1.42748	1.45796
MIDDLE	1.4478	1.4351	1.43764	1.4224	1.4478	1.4605
BOTTOM	1.45796	1.45542	1.4478	1.4478	1.4478	1.45034
FOIL THICKNESS						
TOP	0.29972	0.29972	0.29718	0.29972		
BOTTOM	0.29972	0.29972	0.47752	0.30226		

Table 6: Thickness measurements for L2P16Z [1]

POST IRRADIATION						
TOP	1.449	1.509	1.521	1.531	1.534	1.501
MIDDLE	1.425	1.525	1.534	1.561	1.565	1.536
BOTTOM	1.427	1.526	1.559	1.553	1.559	1.558
PRE-IRRADIATION						
TOP	1.43256	1.45542	1.45288	1.47574	1.4732	1.4224
MIDDLE	1.41478	1.43002	1.45796	1.4732	1.4732	1.45542
BOTTOM	1.4224	1.43002	1.46558	1.4732	1.4732	1.46812
FOIL THICKNESS						
TOP	0.53848	0.5334	0.5334	0.5334		
BOTTOM	0.54102	0.53086	0.52832	0.54102		

Table 7: Thickness measurements for R6R018 [2]

POST IRRADIATION						
TOP	1.447	1.542	1.511	1.492	1.518	1.550
MIDDLE	1.431	1.555	1.511	1.506	1.509	1.559
BOTTOM	1.422	1.686	1.594	1.607	1.591	1.687
PRE-IRRADIATION						
TOP	1.43002	1.4351	1.41478	1.41478	1.4224	1.40462
BOTTOM	1.4224	1.42748	1.41986	1.4224	1.41732	1.41478